

# AIX-MARSEILLE UNIVERSITY

DOCTORAL SCHOOL: Physics and Material Science

PARTENAIRES DE RECHERCHE

Laboratoire MADIREL

Submitted with the view of obtaining the degree of doctor

Discipline: Material Science

Specialty: Characterisation of porous materials

Paul A. Iacomì

Titre de la thèse: sous-titre de la thèse

Defended on JJ/MM/AAAA in front of the following jury:

|            |             |                    |
|------------|-------------|--------------------|
| Prénom NOM | Affiliation | Rapporteur         |
| Prénom NOM | Affiliation | Rapporteur         |
| Prénom NOM | Affiliation | Examineur          |
| Prénom NOM | Affiliation | Examineur          |
| Prénom NOM | Affiliation | Examineur          |
| Prénom NOM | Affiliation | Directeur de thèse |

National thesis number: 2017AIXM0001/001ED62



This work falls under the conditions of the Creative Commons Attribution License - No commercial use - No modification 4.0 International.

# Abstract

Abstract is here.

# Acknowledgements

Acknowledgements go here

# Contents

|   |            |
|---|------------|
| <b>Abstract</b>   | <b>iii</b> |
| <b>Acknowledgements</b>   | <b>iv</b>  |
| <b>1. Building a framework for adsorption data processing</b>             | <b>1</b>   |
| 1.1. Introduction . . . . .   | 1          |
| 1.2. Physical models of adsorption . . . . .                              | 2          |
| 1.2.1. The Henry model . . . . .  | 3          |
| 1.2.2. Langmuir and multi-site Langmuir model . . . . .                   | 3          |
| 1.2.3. BET model . . . . .  | 5          |
| 1.2.4. Toth model . . . . .   | 7          |
| 1.2.5. Temkin model . . . . .   | 7          |
| 1.2.6. Jensen-Seaton model . . . . .                                      | 8          |
| 1.2.7. Quadratic model . . . . .  | 8          |
| 1.2.8. Virial model . . . . .   | 9          |
| 1.2.9. Vacancy solution theory models . . . . .                           | 9          |
| 1.3. Characterisation of materials through adsorption . . . . .           | 10         |
| 1.3.1. Specific surface area and pore volume calculation . . . . .        | 10         |
| 1.3.2. Assessing porosity . . . . .                                       | 14         |
| 1.3.3. Predicting multicomponent adsorption . . . . .                     | 19         |
| 1.4. pyGAPS overview . . . . .  | 21         |
| 1.4.1. Core structure . . . . .   | 21         |
| 1.4.2. Creation of an Isotherm . . . . .                                  | 23         |
| 1.4.3. Units . . . . .  | 25         |
| 1.4.4. Workflow . . . . .   | 25         |
| 1.4.5. Characterisation using pyGAPS . . . . .                            | 26         |
| 1.5. Processing a large adsorption dataset . . . . .                      | 33         |
| 1.5.1. The NIST ISODB dataset . . . . .                                   | 33         |
| 1.5.2. A comparison between surface area calculation methods . . . . .    | 35         |
| 1.5.3. Variability of the dataset . . . . .                               | 35         |
| 1.6. Conclusion . . . . .   | 38         |
| Bibliography . . . . .  | 39         |
| <b>2. Extending bulk analysis of porous compounds through calorimetry</b> | <b>44</b>  |
| 2.1. Introduction . . . . .   | 44         |
| 2.2. Energetics of adsorption . . . . .                                   | 45         |
| 2.2.1. Forces involved in adsorption . . . . .                            | 45         |

|           |   |           |
|-----------|---|-----------|
| 2.2.2.    | Adsorption thermodynamics . . . . .   | 46        |
| 2.2.3.    | Enthalpy of adsorption . . . . .  | 47        |
| 2.2.4.    | Measuring the enthalpy of adsorption . . . . .  | 48        |
| 2.3.      | Methods . . . . .   | 50        |
| 2.3.1.    | Microcalorimetry . . . . .  | 50        |
| 2.4.      | Results and discussion . . . . .  | 50        |
| 2.4.1.    | Routine characterization of a MOF sample . . . . .                                    | 50        |
| 2.4.2.    | Analysis of a carbon sample for gas separation applications . . . . .                 | 51        |
| 2.5.      | Conclusion . . . . .  | 52        |
|           | Bibliography . . . . .  | 53        |
| <b>3.</b> | <b>Exploring the impact of synthesis and defects on adsorption mea-<br/>surements</b> | <b>49</b> |
| 3.1.      | Introduction . . . . .  | 49        |
| 3.2.      | The defective nature of MOFs . . . . .  | 51        |
| 3.2.1.    | Types of crystal defects and their analogues in MOFs . . . . .                        | 51        |
| 3.2.2.    | Consequences of defects . . . . .   | 53        |
| 3.2.3.    | Defect engineering of MOFs . . . . .  | 54        |
| 3.2.4.    | The propensity of UiO-66(Zr) for defect generation . . . . .                          | 54        |
| 3.3.      | Materials and methods . . . . .   | 56        |
| 3.3.1.    | Materials . . . . .   | 56        |
| 3.3.2.    | Methods for quantifying defects . . . . .   | 58        |
| 3.4.      | Results and discussion . . . . .  | 59        |
| 3.4.1.    | Crystallinity of leached samples . . . . .  | 59        |
| 3.4.2.    | NMR . . . . .   | 59        |
| 3.4.3.    | Thermogravimetry results . . . . .  | 59        |
| 3.4.4.    | Nitrogen sorption at 77K . . . . .  | 62        |
| 3.4.5.    | Characterisation of trends . . . . .  | 62        |
| 3.4.6.    | Carbon dioxide isotherms . . . . .  | 68        |
| 3.5.      | Conclusion . . . . .  | 69        |
|           | Bibliography . . . . .  | 70        |
| <b>4.</b> | <b>Exploring the impact of material form on adsorption measurements</b>               | <b>78</b> |
| 4.1.      | Introduction . . . . .  | 78        |
| 4.2.      | Shaping in context . . . . .  | 79        |
| 4.3.      | Materials, shaping and characterisation methods . . . . .                             | 81        |
| 4.3.1.    | Materials . . . . .   | 81        |
| 4.3.2.    | Shaping Procedure . . . . .   | 82        |
| 4.3.3.    | Characterisation of powders and pellets . . . . .                                     | 82        |
| 4.3.4.    | Sample activation for adsorption . . . . .  | 83        |
| 4.4.      | Results and discussion . . . . .  | 83        |
| 4.4.1.    | Thermal stability . . . . .   | 83        |
| 4.4.2.    | Adsorption isotherms at 77K and room temperature . . . . .                            | 83        |
| 4.4.3.    | Room temperature gas adsorption and microcalorimetry . . . . .                        | 86        |

|  |            |
|--|------------|
| 4.4.4. Vapour adsorption . . . . .                 | 92         |
| 4.5. Conclusion . . . . .                          | 99         |
| Bibliography . . . . .                             | 100        |
| <b>5. Exploring novel behaviours</b>               | <b>104</b> |
| 5.1. Introduction . . . . .                        | 104        |
| 5.2. Literature . . . . .                          | 104        |
| 5.3. Method . . . . .                              | 104        |
| 5.4. Results and discussion . . . . .              | 104        |
| 5.5. Conclusion . . . . .                          | 104        |
| Bibliography . . . . .                             | 105        |
| <b>A. Common characterisation techniques</b>       | <b>106</b> |
| A.1. Thermogravimetry . . . . .                    | 106        |
| A.2. Bulk density determination . . . . .          | 106        |
| A.3. Skeletal density determination . . . . .      | 107        |
| A.4. Nitrogen physisorption at 77 K . . . . .      | 107        |
| A.5. Vapour physisorption at 298 K . . . . .       | 107        |
| A.6. Gravimetric isotherms . . . . .               | 108        |
| A.7. High throughput isotherm measuremnt . . . . . | 108        |
| A.8. Powder X-ray diffraction . . . . .            | 108        |
| A.9. Nuclear magnetic resonance . . . . .          | 108        |
| Bibliography . . . . .                             | 108        |
| <b>B. Synthesis method of referenced materials</b> | <b>109</b> |
| B.1. Takeda 5A reference carbon . . . . .          | 109        |
| B.2. MCM-41 controlled pore glass . . . . .        | 109        |
| B.3. Zr fumarate MOF . . . . .                     | 109        |
| B.4. UiO-66(Zr) for defect study . . . . .         | 109        |
| B.5. UiO-66(Zr) for shaping study . . . . .        | 110        |
| B.6. MIL-100(Fe) for shaping study . . . . .       | 110        |
| B.7. MIL-127(Fe) for shaping study . . . . .       | 110        |
| Bibliography . . . . .                             | 111        |
| <b>C. Appendix for chapter 4</b>                   | <b>112</b> |
| C.1. Calorimetry dataset UiO-66(Zr) . . . . .      | 112        |
| C.2. Calorimetry MIL-100(Fe) . . . . .             | 113        |
| C.3. Calorimetry MIL-127(Fe) . . . . .             | 116        |
| Bibliography . . . . .                             | 116        |

## 2. Extending bulk analysis of porous compounds through calorimetry

### 2.1. Introduction

While the previous chapter focused on a physical description of adsorption and its use for the characterisation of porous materials, a rigorous thermodynamic background was omitted. However, an understanding of the energetic aspects of adsorption allows for one of the most powerful applications of adsorption methodology, namely a representation of the kinds of physical and chemical processes occurring during adsorption. Through a direct or indirect measurement of the so-called enthalpy of adsorption ( $h_{ads}$ ), information about surface composition, the strength of adsorbate-guest and guest-guest interactions, phase change phenomena and, in some cases, transitions in the adsorbing material itself can be obtained.

Furthermore, the enthalpy of adsorption is a crucial parameter in an industrial setting. Owing to the exothermic nature of adsorption in combination with the strong influence of temperature on the performance of adsorbent materials,  $h_{ads}$  is often regarded as the most important parameter in the design of beds and columns, alongside working capacity and adsorption/catalytic selectivity. The enthalpy of adsorption is also a measure of the guest-host interactions, which have to be overcome for material regeneration. As such, it represents an important metric of the energy efficiency of the process.

As such the insight afforded through measurement of the energetic components of adsorption can prove invaluable for investigating subtle changes in adsorbent materials which lead to the kind of variability encountered in chapter 1. The thoroughness and suitability of the activation procedure, presence of surface functionalisations, defect formation such as inclusion of counterions and vacancies and activation-driven phenomena such as gate opening, state switching or flexibility all be qualitatively and, with careful methodology, even quantitatively analysed.

### Chapter summary

First, an overview of the theoretical aspects underpinning the energetics of adsorption is presented. The methods section will go into detail in the available methodology for studying the enthalpy of adsorption on surfaces and in pores. The final part of the chapter will explore the use of combined adsorption and calorimetric measurements as a way of extending characterisation of porous materials.



## Contributions

The sample of Zr Fumarate MOF was synthesised in the group of Prof. Peter Behrens, from the University of Hannover, Germany. All presented measurements and data processing were performed by Paul Iacomini in the Madirel Laboratory, Marseille.

## 2.2. Energetics of adsorption

### 2.2.1. Forces involved in adsorption

From a classical molecular point of view, we can define the guest-host and guest-guest interactions as a sum of several components with distinct physical meaning.

$$\Phi_t = \Phi_R + \Phi_D + \Phi_C + \Phi_I \quad (2.1)$$

The first two types of interaction, namely short range electrostatic repulsion between the electron clouds of neighbouring atoms  $\Phi_R$  and long range dispersion  $\Phi_D$  arising from incidental short-lived partial charges are common to all atoms, and can therefore be called “non-specific”. Such interactions are commonly modelled through the use of a Lennard-Jones type potential function.

$$V_{LJ} = 4\epsilon \left[ \left( \frac{\sigma}{r} \right)^{12} - \left( \frac{\sigma}{r} \right)^6 \right] \quad (2.2)$$

The latter two types, Coulombic interactions  $\Phi_C$  and induction interactions  $\Phi_I$  arise from permanent charges and multipoles in the system. Coulombic interactions are attraction and repulsion interactions between charges such as molecular ions, permanent dipoles and quadrupoles. Induction, also known as polarization or Debye forces, is the interaction between a charged particle or a multipole with the induced multipole in a non-charged system. The ease of inducing such an interaction in a molecule is termed polarizability. These interactions can be referred to as “specific”.

Therefore, in the standard definition of adsorption, only Van-der-Waals forces are responsible. However, depending on the systems involved, stronger interactions such as hydrogen bonding, electron sharing, stacking or  $\pi$  interactions may also play a role in the overall stability of the guest-host attraction.

The total interactions can also be broken down as contributions from guest-host interactions and guest-guest interactions. If changes in the adsorbent occur as a result of adsorption, a host-host or self-potential interaction should be considered. The guest-host interaction can be assumed constant for a homogeneous surface or a function of coverage, in the case of a heterogeneous surface.

Unfortunately, only the total sum of all interactions is measurable through direct methods. Therefore, the absolute contribution of each component is unknowable unless computational methods are employed.

### 2.2.2. Adsorption thermodynamics

As mentioned in the previous section, adsorption is a consequence of intermolecular attraction between the material surface and the molecules of the fluid. The sum of all interactions accounts for the depth of the potential well and therefore for the energy corresponding to the process. As this energy is net positive, adsorption is an overall exothermic phenomenon.

However, in order to make the transition from a molecular viewpoint to a macroscale bulk fluid representation of adsorption, the a thermodynamic description of the adsorbed phase of the process must be performed.

#### The Gibbs surface excess approach

A description of the adsorbed phase can be made through expressing the change in density or concentration of fluid from the adsorbent surface to the bulk phase. The density has a maxima in the immediate zone close to the surface, and then decreases until it reaches the density of the bulk fluid. However, when defined as such, the boundary between the two phases is difficult to pinpoint. Therefore, in most cases it is useful to employ the concept of the Gibbs dividing surface.

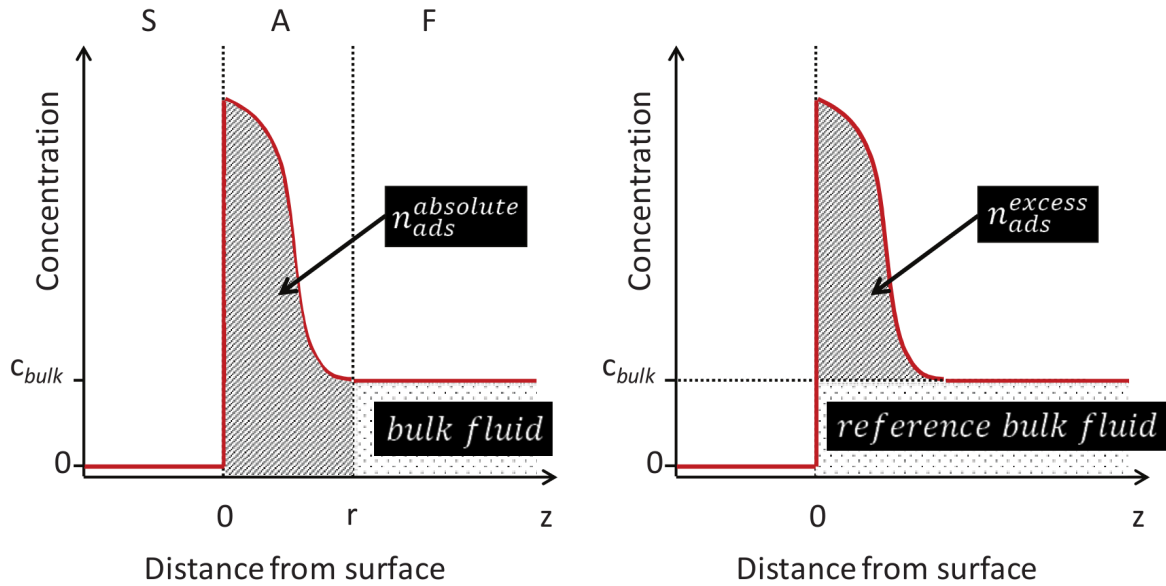


Figure 2.1.: Representation of the adsorbed and bulk phases according to the (left) layer model and the (right) Gibbs dividing surface approach. Adapted from Rouquerol et al..<sup>(1)</sup>

This approach describes the adsorbed phase only in terms of an *excess* from the properties of the bulk phase. As represented in Figure 2.1, the total amount adsorbed

## 2. Extending bulk analysis of porous compounds through calorimetry

can be defined as:

$$n_{ads}^{absolute} = A \int_0^r c \, dz \quad (2.3)$$

The imaginary Gibbs dividing surface is usually placed parallel to the real surface of the adsorbent and in the resulting system, the concentration of the adsorbent in the adsorbed phase are expressed as an excess from the concentration of the bulk fluid. The relationship between the total amount adsorbed and the excess amount adsorbed is then:

$$n_{ads}^{excess} = n_{ads}^{absolute} + V_{ads} \cdot c_{bulk} \quad (2.4)$$

As long as the volume of the adsorbed layer  $V_{ads}$  can be considered negligible and the concentration of adsorbate in the bulk phase  $c_{bulk}$  is low, the total amount adsorbed and the surface excess amount may be considered as approximately equal. At high pressures or when the difference in concentration between the adsorbed and the bulk phase is low, the total amount adsorbed begins to diverge significantly from the surface excess.

Without corrections, both the gravimetric and manometric method of adsorption will measure excess amounts adsorbed. In the case of adsorption in porous materials, the volume of the adsorbed phase may be taken as total pore volume.

### 2.2.3. Enthalpy of adsorption

Adsorption can be considered as a closed system of constant volume  $V$  and temperature  $T$ . No mass of material crosses the system boundary, therefore the change in chemical potential is also zero  $d\mu = 0$ . The Helmholtz free energy is used for a description of the thermodynamic potential of such as system.

The differential enthalpy of adsorption is then the change of the total enthalpy with respect to the number of moles adsorbed at a certain equilibrium pressure and surface concentration. It is given by:

$$\Delta_{ads} \dot{h} = \quad (2.5)$$

The differential enthalpy of adsorption is often represented as a function of partial coverage. In Figure 2.2, isotherm types as defined by IUPAC are presented together with a typical differential enthalpy curve. Type I isotherms often have an initial plateau, corresponding to adsorption in micropores until a sharp decrease at complete pore filling occurs. If the surface of the pores is heterogeneous, higher energy sites will be occupied first, resulting in a sharp slope at low loadings. Multilayer adsorption in non-porous or mesoporous materials (II and IV) yields a slowly decreasing enthalpy curve, as the solid-guest interactions drop off with increasing layers adsorbed. Finally, cooperative adsorption, as seen in a type III isotherm, often gives rise to initial enthalpies of adsorption which are below the enthalpy of vaporisation. It should be noted that changes in the adsorbed fluid similar to phase changes may occur, which can be seen in the enthalpy curve as a distinct peak.<sup>(2,3)</sup>

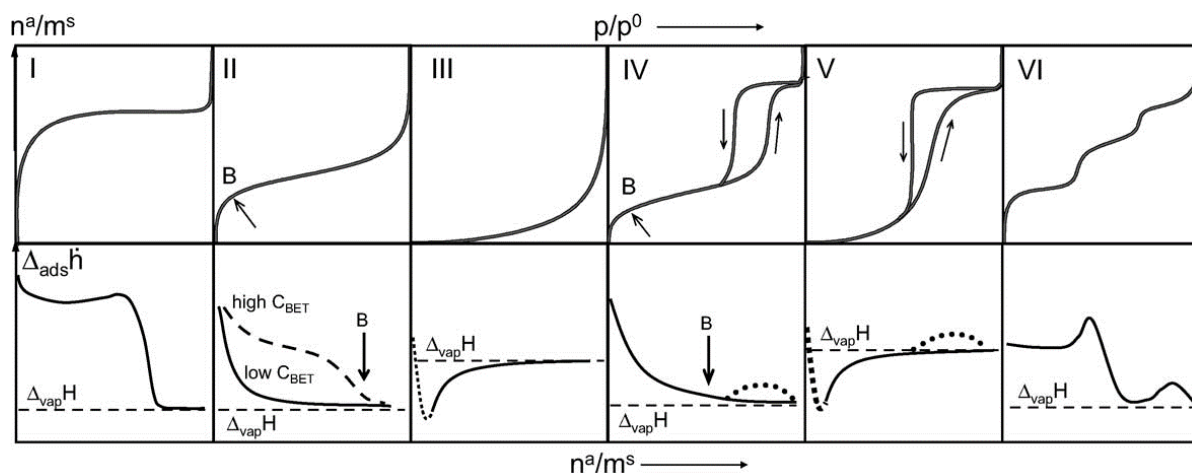


Figure 2.2.: Generalized curves of differential enthalpy of adsorption with respect to coverage corresponding to different IUPAC-defined isotherm types. Adapted from Llewellyn and Maurin.<sup>(4)</sup>

## 2.2.4. Measuring the enthalpy of adsorption

Experimentally, two methods are widely used for determining the enthalpy of adsorption. The first relies on the applicability of the Clausius-Clapeyron equation to two or more isotherms measured at different temperatures while the second is a direct measurement of the evolved heat during adsorption using calorimetry.

A value for the enthalpy of adsorption in a particular system may also be obtained from computer simulation methods. The accuracy of these procedures depends on the accuracy of the chosen model of interaction between simulated molecules.

### Isosteric enthalpy of adsorption

The isosteric enthalpy of adsorption is calculated from experimental data using the Clausius-Clapeyron equation as the starting point:

$$\left(\frac{\partial \ln P}{\partial T}\right)_{n_a} = -\frac{\Delta H_{ads}}{RT^2} \quad (2.6)$$

Where  $\Delta H_{ads}$  is the isosteric enthalpy of adsorption. If it is assumed that the adsorption enthalpy does not vary with temperature, the equation can be rearranged to:

$$\Delta H_{ads} = -R \frac{\partial \ln P}{\partial 1/T} \quad (2.7)$$

In order to approximate the partial differential, two or more isotherms are measured at different temperatures. Afterwards the isosteric enthalpy of adsorption can be calculated by using the pressures at which the loading is identical using the rearranged equation.

## 2. Extending bulk analysis of porous compounds through calorimetry

By plotting the values of  $\ln P$  against  $1/T$  we should obtain a straight line with a slope of  $-\Delta H_{ads}/R$ .

The isosteric enthalpy is sensitive to the differences in pressure between the two isotherms. If the isotherms measured are too close together, the error margin will increase. The method also assumes that isosteric enthalpy does not vary with temperature. If the variation is large for the system in question, the calculation will give unrealistic values.


Even with carefully measured experimental data, there are two assumptions used in deriving the Clausius-Clapeyron equation: an ideal bulk gas phase and a negligible adsorbed phase molar volume. These have a significant effect on the calculated isosteric enthalpy of adsorption, especially at high relative pressures and for heavy adsorbates.

### Microcalorimetry

A direct measurement of the enthalpy of adsorption is possible using calorimetric methods.

For the best performance, a 3D Tian-Calvet thermopile is used, which allows for a complete integration of evolved heat.

Two options exist, based on two methods of obtaining adsorption isotherms: the continuous and the discontinuous or point-by-point method. In the point-by-point method, discrete steps of introduction of adsorbate are taken. A reference volume is filled with gas at a pressure  $p$ , which is allowed to equilibrate before a valve between the reference volume and the cell containing the adsorbate. In the other method, the flow of adsorbate is continuous, usually kept constant by a restriction in the pipe diameter which is severe enough to enter sonic flow regimes. At this point, the flowrate is no longer influenced by a pressure differential, instead becoming a function only of upstream pressure and environment temperature.

The heat generated during adsorption (or required during desorption) is therefore measured either as discrete peaks, corresponding to each event or as a continuous heat curve. An example of such a signal is presented in 

The point-by-point method is less accurate than a continuous introduction, as the measured heat is necessarily a cumulative value of instantaneous differential enthalpy for the coverage range of each adsorbed point. However, it has the advantage of ensuring complete equilibrium at each step, by observing the return to the baseline of the calorimetry signal, or no changes in the pressure signal. On the other hand, the continuous method allows for subtle changes in the enthalpy of adsorption, such as those corresponding to adsorbed phase ordering or changes, to be seen experimentally. Additionally, the time-resolved data can be used to investigate transient phenomena. Equilibrium between the adsorbed phase and gas phase is no longer assured, and must be tested for by performing multiple experiments at different adsorbate flowrates. Alternatively, the experiment can be stopped to observe that the time for the heat signal to return to its baseline does not diverge from the dead time of the calorimeter.

The heat value which is measured through calorimetry corresponds to two components, the differential enthalpy of adsorption and the work required to expand the gas into the

## 2. Extending bulk analysis of porous compounds through calorimetry

measurement cell. In this relationship as expressed in Equation 2.8 the value for work can be substituted by  $V\Delta P$  and accounted for at each point.

$$\dot{Q} = \Delta_{ads}h + W \quad (2.8)$$

$$\dot{Q} = \Delta_{ads}h + V\Delta P \quad (2.9)$$

$$\Delta_{ads}h = \dot{Q} - V\Delta P \quad (2.10)$$

Finally, to obtain a value for the differential enthalpy of adsorption, the enthalpy is divided by the amount of gas adsorbed in the same time.

## 2.3. Methods

### 2.3.1. Microcalorimetry

In this thesis, combined isotherms and enthalpy of adsorption measurements were made experimentally using a Tian-Calvet type microcalorimeter coupled with a home-made manometric gas dosing system.<sup>(4)</sup> This apparatus allows the simultaneous measurement of the adsorption isotherm and the corresponding differential enthalpies. Gas is introduced into the system using a step-by-step method and each dose is allowed to stabilize in a reference volume before being brought into contact with the adsorbent located in the microcalorimeter. The introduction of the adsorbate to the sample is accompanied by an exothermic thermal signal, measured by the thermopiles of the microcalorimeter. The peak in the calorimetric signal is integrated over time to give the total energy released during this adsorption step. At low coverage the error in the signal can be estimated to around  $\pm 0.2 \text{ kJ mol}^{-1}$ . Around 0.4 g of sample is used in each experiment. For each injection of gas, equilibrium was assumed to have been reached after 90 minutes. This was confirmed by the return of the calorimetric signal to its baseline ( $<5 \text{ } \mu\text{W}$ ).

### Data processing

## 2.4. Results and discussion

### 2.4.1. Routine characterization of a MOF sample

New materials are often screened for their ability to act as a  $\text{CO}_2$  capture material. A good predictor of performance in this application are the enthalpies of adsorption, which are an indication of host-guest interactions. Here, we first measure the differential heats of adsorption directly through the use of adsorption microcalorimetry at 303 K. Then, to determine the isosteric heats of adsorption, two isotherms have been measured at 303 K and 323 K respectively. The complete set of isotherms is loaded into `pyGAPS` and plotted by the `pygaps.plot_iso()` function as seen in Figure ???. To calculate the isosteric heat of adsorption, the two isotherms measured for this purpose are passed through the

## 2. Extending bulk analysis of porous compounds through calorimetry

`pygaps.isosteric_heat()` function. The results from the calculation are overlaid on top of the measured calorimetric data in Figure ???. The two datasets are overlap for the most part but diverge at low loadings and near complete coverage. At low loading the small changes in pressure amount introduce large errors in the Clausius-Clapeyron equation. This, together with the breakdown of the assumption of equilibrium due to active sites in the MOF lead to the calorimetric measurement providing more valid results. At higher loadings, where the isotherm reaches a plateau and the change in adsorbed amount is small from point to point, errors are introduced in the direct calculation of the heat of adsorption. The two techniques are thus complementary.

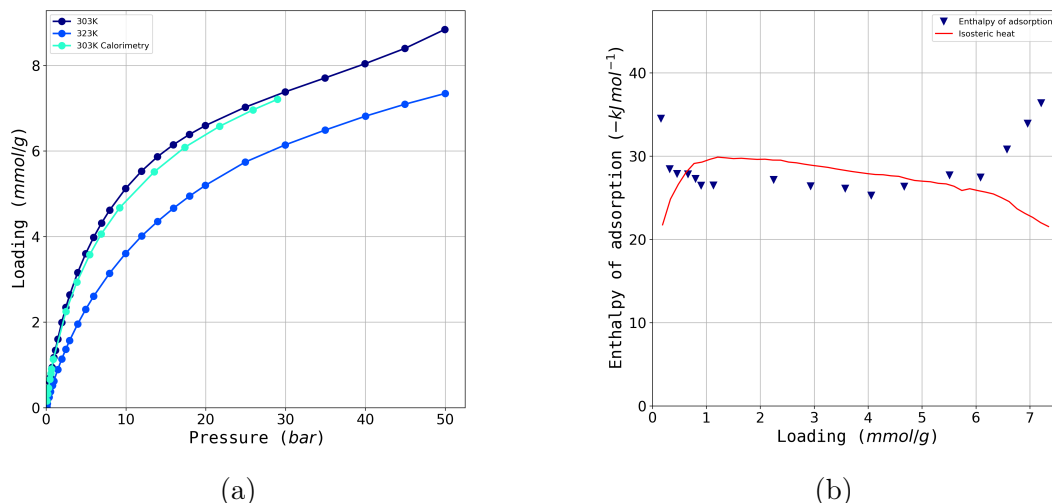


Figure 2.3.: Calculation of enthalpy of adsorption: (a) the dataset of isotherms used and (b) the calculated isosteric heat (red line) together with the measured differential enthalpy of adsorption (blue triangles)

### 2.4.2. Analysis of a carbon sample for gas separation applications

A sample of reference carbon Takeda 5A is to be investigated for an in-depth characterisation of the adsorption behaviour of pure gases, with a focus on describing the pore environment. Afterwards, the performance of different binary separations is evaluated, such as  $CO_2/N_2$  and propane/propylene.

Pure gas adsorption data has been recorded at 303 K in conjunction with microcalorimetry on  $N_2$ ,  $CO$ ,  $CO_2$ ,  $CH_4$ ,  $C_2H_6$ ,  $C_3H_6$  and  $C_3H_8$ . The complete dataset is plotted with the `pygaps.plot_iso()` function and can be seen in Figure 2.4a.

Nitrogen and carbon monoxide are similar in their adsorption behaviour, with a nearly linear isotherm and low capacities. Hydrocarbons are adsorbed with higher loadings, with both propane and propylene reaching a plateau at low pressures. Propylene is seen to have a higher capacity than propane, with packing effects as a likely cause. Carbon dioxide has the highest loading capacity of the entire dataset.

## 2. Extending bulk analysis of porous compounds through calorimetry

Two parameters can be useful in characterising the local pore environment before guest-guest interactions come into effect: the Henry constant at low loadings as well as the initial enthalpy of adsorption. Both can be calculated with `pyGAPS`, with several options in regard to the methodology. Here, Henry’s constant is calculated using the `pygaps.initial_henry_virial()` function, which fits a virial model to the isotherm and then takes the limit at loading approaching zero. The initial enthalpy of adsorption is obtained through the `pygaps.initial_enthalpy_comp()` function. This fits the enthalpy curve to a compound contribution from guest-host interaction, defects, guest-guest attraction and repulsion using a minimization algorithm. The results of the calculations are plotted versus the polarizability of the gas used, which can be obtained from the respective `Adsorbate` class. Figure 2.4b shows that both the parameters fall on a linear trend, which suggests that the interactions between those guests and the pore walls are mostly due to Lennard-Jones interactions. Carbon dioxide has a higher enthalpy of adsorption than the baseline due to the contribution from its quadrupole moment. There is almost a complete overlap between propane and propylene, which leads to the conclusion that the unsaturated double bond does not interact in a specific way with the carbon surface. The difference between the two isotherms is due exclusively to steric and packing effects.

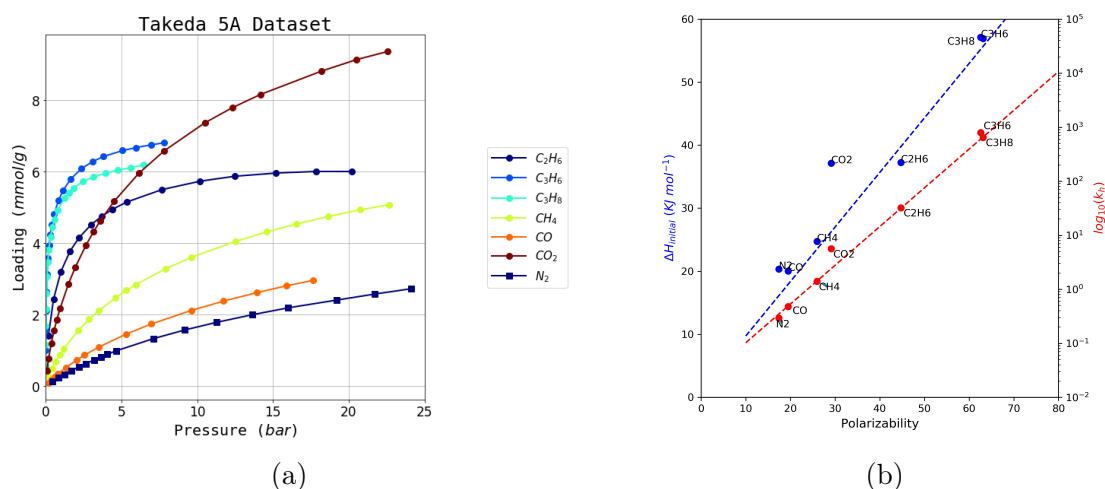


Figure 2.4.: Takeda 5A dataset processing: (a) the experimental dataset all recorded gases and (b) the calculated trends of initial heat of adsorption and Henry’s constant

## 2.5. Conclusion



## Bibliography

- [1] Jean Rouquerol, Françoise Rouquerol, Philip L. Llewellyn, Guillaume Maurin, and Kenneth Sing. *Adsorption by Powders and Porous Solids : Principles, Methodology and Applications*. 2013. ISBN 978-0-08-097035-6.
- [2] P. L. Llewellyn, J. P. Coulomb, Y. Grillet, J. Patarin, H. Lauter, H. Reichert, and J. Rouquerol. Adsorption by MFI-type zeolites examined by isothermal microcalorimetry and neutron diffraction. 1. Argon, krypton, and methane. *Langmuir*, 9(7):1846–1851, July 1993. ISSN 0743-7463, 1520-5827. doi: 10.1021/la00031a036.
- [3] P. L. Llewellyn, J. P. Coulomb, Y. Grillet, J. Patarin, G. Andre, and J. Rouquerol. Adsorption by MFI-type zeolites examined by isothermal microcalorimetry and neutron diffraction. 2. Nitrogen and carbon monoxide. *Langmuir*, 9(7):1852–1856, July 1993. ISSN 0743-7463, 1520-5827. doi: 10.1021/la00031a037.
- [4] Philip L. Llewellyn and Guillaume Maurin. Gas adsorption microcalorimetry and modelling to characterise zeolites and related materials. *Comptes Rendus Chimie*, 8(3-4):283–302, March 2005. ISSN 16310748. doi: 10.1016/j.crci.2004.11.004.

# A. Common characterisation techniques

pictures?

## A.1. Thermogravimetry

Thermogravimetry (TGA) is a standard laboratory technique where the weight of a sample is monitored while ambient temperature is controlled. Changes in sample mass can be correlated to physical events, such as adsorption, desorption, sample decomposition or oxidation, depending on temperature and its rate of change.

TGA experiments are carried out on approximately 15 mg of sample with a TA Instruments Q500 up to 800 °C. The sample is placed on a platinum crucible and sealed in a temperature controlled oven, under gas flow of 40 cm<sup>3</sup> min<sup>-1</sup>. Experiments can use a blanket of either air or argon. The temperature ramp can be specified directly and should be chosen to ensure that the sample is in equilibrium with the oven temperature and no thermal conductivity effects come into play. Alternatively, a dynamic “Hi-Res” mode can be used which allows for automatic cessation of heating rate while the sample undergoes mass loss.

The main purpose of thermogravimetry as used in this thesis is the determination of sample decomposition temperature, to ensure that thermal activation prior to adsorption is complete and that all guest molecules have been removed without loss of structure. To this end, experiments are performed under an inert atmosphere (argon), and the sample activation temperature is chosen as 50 °C to 100 °C lower than the sample decomposition temperature.

## A.2. Bulk density determination

Bulk density is a useful metric for the industrial use of adsorbent materials, as their volume plays a critical role in equipment sizing.

Bulk density is determined by weighing 1.5 ml empty glass vessels and settling the MOFs inside. Powder materials are then added in small increments and settled through vibration between each addition. The full vessel is finally weighed, which allowed the bulk density to be determined. The same cell is used in all experiments, with cleaning through sonication between each experiment.

### **A.3. Skeletal density determination**

True density or skeletal density is determined through gas pycnometry in a MicrotracBEL BELSORP-max apparatus. Helium is chosen as the fluid of choice as it is assumed to be non-adsorbing.

The volume of a glass sample cell ( $V_c$ ) is precisely measured through dosing of the reference volume with helium up to ( $p_1$ ), then opening the valve connecting the two and allowing the gas to expand up to ( $p_2$ ). Afterwards approximately 50 mg of sample are weighed and inserted in a glass sample cell. After sample activation using the supplied electric heater to ensure no solvent residue is left in the pores, the same procedure is repeated to determine the volume of the cell and the adsorbent. With the volume of the sample determined, the density can be calculated by.

$$V_s = V_c + \frac{V_r}{1 - \frac{p_1}{p_2}} \quad (\text{A.1})$$

### **A.4. Nitrogen physisorption at 77 K**

Nitrogen adsorption experiments are carried out on a Micromeritics Triflex apparatus. Approximately 60 mg of sample are used for each measurement. Empty glass cells are weighed and filled with the samples, which are then activated in a Micromeritics Smart VacPrep up to their respective activation temperature under vacuum and then back-filled with an inert atmosphere. After sample activation, the cells are re-weighed to determine the precise sample mass. The cells are covered with a porous mantle which allows for a constant temperature gradient during measurement by wicking liquid nitrogen around the cell. Finally, the cells are immersed in a liquid nitrogen bath and the adsorption isotherm is recorded using the volumetric method. A separate cell is used to condense the adsorptive throughout the measurement for accurate determination of its saturation pressure.

### **A.5. Vapour physisorption at 298 K**

Vapour adsorption isotherms throughout this work are measured using a MicrotracBEL BELSORP-max apparatus in vapour mode. Glass cells are first weighed and then filled with about 50 mg of sample. The vials are then heated under vacuum up to the activation temperature of the material and re-weighed in order to measure the exact sample mass without adsorbed guests. The cells are then immersed in a mineral oil bath kept at 298 K. To ensure that the cold point of the system occurs in the material and to prevent condensation on cell walls, the reference volume, dead space and vapour source are temperature controlled through an insulated enclosure.

## A.6. Gravimetric isotherms

The gravimetric isotherms in this thesis are obtained using a commercial Rubotherm GmbH balance. Approximately 1 g of dried sample is used for these experiments. Samples are activated in situ by heating under vacuum. The gas is introduced using a step-by-step method, and equilibrium is assumed to have been reached when the variation of weight remained below 30  $\mu\text{g}$  over a 15 min interval. The volume of the sample is determined from a blank experiment with helium as the non-adsorbing gas and used in combination with the gas density measured by the Rubotherm balance to compensate for buoyancy.

## A.7. High throughput isotherm measurement

A high-throughput gas adsorption apparatus is presented for the evaluation of adsorbents of interest in gas storage and separation applications. This instrument is capable of measuring complete adsorption isotherms up to 50 bar on six samples in parallel using as little as 60 mg of material. Multiple adsorption cycles can be carried out and four gases can be used sequentially, giving as many as 24 adsorption isotherms in 24 h.<sup>(1)</sup>

## A.8. Powder X-ray diffraction

## A.9. Nuclear magnetic resonance

## Bibliography

- [1] Andrew D. Wiersum, Christophe Giovannangeli, Dominique Vincent, Emily Bloch, Helge Reinsch, Norbert Stock, Ji Sun Lee, Jong-San Chang, and Philip L. Llewellyn. Experimental Screening of Porous Materials for High Pressure Gas Adsorption and Evaluation in Gas Separations: Application to MOFs (MIL-100 and CAU-10). *ACS Combinatorial Science*, 15(2):111–119, February 2013. ISSN 2156-8952. doi: 10.1021/co300128w.

## B. Synthesis method of referenced materials

### B.1. Takeda 5A reference carbon

The Takeda 5A carbon was purchased directly from the Takeda corporation. The sample was activated at 250 °C under secondary vacuum (5 mbar) before any measurements.

full  
char-  
acteri-  
zation

### B.2. MCM-41 controlled pore glass

MCM-41 (Mobil Composition of Matter No. 41) is a mesoporous silica ( $\text{SiO}_2$ ) material with a narrow pore distribution. First synthesised by the Mobil Oil Corporation, it is produced through templated synthesis using mycelle-forming surfactants. The material referenced in this thesis was purchased from Sigma-Aldrich. The activation procedure consists of heating at 250 °C under secondary vacuum (5 mbar).

### B.3. Zr fumarate MOF

The synthesis of the Zr fumarate was performed in Peter Behren's group in Hannover, through modulated synthesis. This MOF can only be synthesised through the addition of a modulator, in this case fumaric acid, to the ongoing reactor, as detailed in the original publication.<sup>(1)</sup>

The procedure goes as follows:  $\text{ZrCl}_4$  (0.517 mmol, 1 eq) and fumaric acid (1.550 mmol, 3 eq) are dissolved in 20 mL N,N-dimethylformamide (DMF) and placed in a 100 mL glass flask at room temperature. 20 equivalents of formic acid were added. The glass flasks were Teflon-capped and heated in an oven at 120 °C for 24 h. After cooling, the white precipitate was washed with 10 mL DMF and 10 mL ethanol, respectively. The washing process was carried out by centrifugation and redispersion of the white powder, which was then dried at room temperature over night

### B.4. UiO-66(Zr) for defect study

The UiO-66(Zr) sample preparation was adapted from Shearer et al.<sup>(2)</sup> as follows:  $\text{ZrCl}_4$  (1.55 g, 6.65 mmol), an excess of terephthalic acid (BDC) (1.68 g, 10.11 mmol), HCl 37 % solution (0.2 mL, 3.25 mmol) and N,N'-dimethylformamide (DMF) (200 mL,

2.58 mol) were added to a 250 mL pressure resistant Schott bottle. The mixture was stirred for 10 min, followed by incubation in a convection oven at 130 °C for 24 h. The resulting white precipitate was washed with fresh DMF (3× 50 mL) followed by ethanol (3× 50 mL) over the course of 48 h and dried at 60 °C. After drying, the sample was activated on a vacuum oven by heating at 200 °C under vacuum for 12 h. The yield was 78 % white microcrystalline powder. Before the experiment, the sample was calcined at 200 °C under vacuum (5 mbar) to remove any residual solvents from the framework.

## **B.5. UiO-66(Zr) for shaping study**

The scaled-up synthesis of UiO-66(Zr) was carried out in a 5 L glass reactor (Reactor Master, Syrris, equipped with a reflux condenser and a Teflon-lined mechanical stirrer) according to a previously reported method.<sup>(3)</sup> In short, 462 g (2.8 mol) of H<sub>2</sub>BDC (98%) was initially dissolved in 2.5 L of dimethyl formamide (DMF, 2.36 kg, 32.3 mol) at room temperature. Then, 896 g (2.8 mol) of ZrOCl<sub>2</sub> · 8H<sub>2</sub>O (98%) and 465 mL of 37% HCl (548 g, 15 mol) were added to the mixture. The molar ratio of the final ZrOCl<sub>2</sub> · 8H<sub>2</sub>O/H<sub>2</sub>BDC/DMF/HCl mixture was 1 : 1 : 11.6 : 5.4. The reaction mixture was vigorously stirred to obtain a homogeneous gel. The mixture was then heated to 423 K at a rate of 1 K min<sup>-1</sup> and maintained at this temperature for 6 h in the reactor without stirring, leading to a crystalline UiO-66(Zr) solid. The resulting product (510 g) was recovered from the slurry by filtration, redispersed in 7 L of DMF at 333 K for 6 h under stirring, and recovered by filtration. The same procedure was repeated twice, using methanol (MeOH) instead of DMF. The solid product was finally dried at 373 K overnight.

## **B.6. MIL-100(Fe) for shaping study**

The synthesis of the MOF for the shaping study was done at the KRICT institute using a previously published method.<sup>(4)</sup> To synthesise the MIL-100(Fe) material Fe(NO<sub>3</sub>)<sub>3</sub> was completely dissolved in water. Then, trimesic acid (BTC) was added to the solution; the resulting mixture was stirred at room temperature for 1 h. The final composition was Fe(NO<sub>3</sub>)<sub>3</sub> · 9 H<sub>2</sub>O:0.67 BTC:*n* H<sub>2</sub>O (*x*= 55–280). The reactant mixture was heated at 433 K for 12 h using a Teflon-lined pressure vessel. The synthesized solid was filtered and washed with deionized (DI) water. Further washing was carried out with DI water and ethanol at 343 K for 3 h and purified with a 38 mM NH<sub>4</sub>F solution at 343 K for 3 h. The solid was finally dried overnight at less than 373 K in air.

## **B.7. MIL-127(Fe) for shaping study**

MIL-127(Fe) was synthesized by reaction of Fe(ClO<sub>4</sub>)<sub>3</sub> · 6 H<sub>2</sub>O (3.27 g, 9.2 mmol) and C<sub>16</sub>N<sub>2</sub>O<sub>8</sub>H<sub>6</sub> (3.3 g) in DMF (415 mL) and hydrofluoric acid (5 M, 2.7 mL) at 423 K in a Teflon flask. The obtained orange crystals were placed in DMF (100 mL) and

stirred at ambient temperature for 5 h. The final product was kept at 375 K overnight. MIL-127(Fe) was synthesized by reaction of  $\text{Fe}(\text{ClO}_4)_3 \cdot 6 \text{H}_2\text{O}$  (3.27 g, 9.2 mmol) and  $\text{C}_{16}\text{N}_2\text{O}_8\text{H}_6$  (3.3 g) in DMF (415 mL) and hydrofluoric acid (5 M, 2.7 mL) at 423 K in a Teflon flask. The obtained orange crystals were placed in DMF (100 mL) and stirred at ambient temperature for 5 h. The final product was kept at 375 K overnight.

## Bibliography

- [1] Gesa Wißmann, Andreas Schaate, Sebastian Lilienthal, Imke Bremer, Andreas M. Schneider, and Peter Behrens. Modulated synthesis of Zr-fumarate MOF. *Microporous and Mesoporous Materials*, 152:64–70, April 2012. ISSN 13871811. doi: 10.1016/j.micromeso.2011.12.010.
- [2] Greig C. Shearer, Sachin Chavan, Jayashree Ethiraj, Jenny G. Vitillo, Stian Svelle, Unni Olsbye, Carlo Lamberti, Silvia Bordiga, and Karl Petter Lillerud. Tuned to Perfection: Ironing Out the Defects in Metal–Organic Framework UiO-66. *Chemistry of Materials*, 26(14):4068–4071, July 2014. ISSN 0897-4756, 1520-5002. doi: 10.1021/cm501859p.
- [3] Florence Ragon, Patricia Horcajada, Hubert Chevreau, Young Kyu Hwang, U-Hwang Lee, Stuart R. Miller, Thomas Devic, Jong-San Chang, and Christian Serre. In Situ Energy-Dispersive X-ray Diffraction for the Synthesis Optimization and Scale-up of the Porous Zirconium Terephthalate UiO-66. *Inorganic Chemistry*, 53(5):2491–2500, March 2014. ISSN 0020-1669, 1520-510X. doi: 10.1021/ic402514n.
- [4] Felix Jeremias, Stefan K. Henninger, and Christoph Janiak. Ambient pressure synthesis of MIL-100(Fe) MOF from homogeneous solution using a redox pathway. *Dalton Transactions*, 45(20):8637–8644, 2016. ISSN 1477-9226, 1477-9234. doi: 10.1039/C6DT01179A.